A new morphodynamic instability associated to the cross-shore transport in the nearshore

Albert Falqués[1], Francesca Ribas[2], Anna Mujal-Colilles[3], and Càrol Puig-Polo[4]

[1]UPC
[2]Universitat Politecnica de Catalunya, Physics Department
[3]Universitat Politècnica de Catalunya, Department of Nautical Sciences and Engineering
[4]Division of Geotechnical Engineering and Geosciences, Department of Civil and Environmental Engineering, UPC BarcelonaTECH

November 23, 2022

Abstract

The existing theory for alongshore rhythmic bars relies on morphodynamic instabilities involving the wave-driven longshore current and rip currents. Transverse finger bars are common on coasts with a beach profile above the equilibrium profile (something not related to those currents). Here we show that under these conditions, the cross-shore transport can induce an instability which is triggered by the onshore transport together with wave refraction by the emerging bars. It is a finite amplitude instability, something not previously found in coastal geomorphology. We use a numerical model that filters out the dynamics associated to those currents. The alongshore spacing scales with the wavelength of the incident waves and the cross-shore extent is about the distance from shore to the depth of closure. The modelled bars compare qualitatively well with observations at El Trabucador back-barrier beach (Ebro delta, Western Mediterranean Sea).

A new morphodynamic instability associated to the cross-shore transport in the nearshore

A. Falqués[1], F. Ribas[1], A. Mujal-Colilles[2] and C. Puig-Polo[3]

[1]Physics Department, Universitat Politècnica de Catalunya, Campus Diagonal Nord, C. Jordi Girona, 1-3, 08034 Barcelona, Catalonia, Spain
[2]Department of Nautical Sciences and Engineering, Universitat Politècnica de Catalunya
[3]Department of Civil and Environmental Engineering, Universitat Politècnica de Catalunya

Key Points:

- The cross-shore sediment transport in the nearshore can be unstable in the alongshore direction
- The morphodynamic instability can develop only for beach profiles above the equilibrium profile
- This instability could explain transverse bar formation in shallow terraces at back-barrier beaches

Corresponding author: A. Falqués, albert.falques@upc.edu

Abstract

The existing theory for alongshore rhythmic bars relies on morphodynamic instabilities involving the wave-driven longshore current and rip currents. Transverse finger bars are common on coasts with a beach profile above the equilibrium profile (something not related to those currents). Here we show that under these conditions, the cross-shore transport can induce an instability which is triggered by the onshore transport together with wave refraction by the emerging bars. It is a finite amplitude instability, something not previously found in coastal geomorphology. We use a numerical model that filters out the dynamics associated to those currents. The alongshore spacing scales with the wavelength of the incident waves and the cross-shore extent is about the distance from shore to the depth of closure. The modelled bars compare qualitatively well with observations at El Trabucador back-barrier beach (Ebro delta, Western Mediterranean Sea).

Plain Language Summary

Beaches sometimes exhibit sand ridges (bars) nearly perpendicular to the shore that tend to be quite regularly spaced alongshore. Their spacing and cross-shore extent range from tens to thousands of meters. Intriguingly, these bars develop preferably at beaches with an abundant supply of sand such as delta barrier beaches, barrier islands and estuaries. Here we provide a possible explanation. Due to the sand excess, the bed in these beaches is very flat, the tendency for the sand to move downslope is very weak and the waves push the sand onshore. On the other hand, the waves refract, that is, their crest tip on deeper water propagates faster than the tip on shallower water. As a result, they turn towards the shallower areas and, thus, the onshore movement of the sand is deflected towards incipient shoals and accumulates there. This causes more intense wave refraction, which in turn brings more sand to the shallows, and so on. In this way, the bars can form out of small random irregularities in bed level.

1 Introduction

The beach morphology dynamics is the result of the interaction of water motion and sediment over a geological substratum. Coastal sediment transport is still poorly understood so that it largely relies on simplifications and parameterisations (Amoudry & Souza, 2011). At length scales comparable to the surf zone width or larger ($> 10-100$ m) the sediment transport can be conceptually decomposed into two main components. The *longshore transport* is driven by the surf-zone longshore current generated by breaking waves if they approach obliquely to the coast. The *cross-shore transport* is the main cause of the cross-shore beach profile sloping up onshore, sometimes with shore parallel sand bars. The main sources of cross-shore transport are the onshore transport driven by wave asymmetry and skewness, the offshore transport due to the undertow (bed-return current) and the downslope transport due to gravity (Fernández-Mora et al., 2015). An equilibrium bed profile is achieved if the three components are in balance. Finally, there are more contributions to sediment transport that do not fall into the longshore or cross-shore categories (e.g., those associated to the rip current circulation or to low frequency motions).

At sandy coasts, beach morphology is rarely uniform along the coast. Typically, the shoreline has undulations and the nearshore sea bed features shallows and deeps alongshore. Transverse bar systems (Ribas et al., 2015) are a well-known example encompassing a series of shallows or bars separated by deeps called rip channels (Figure 1). These systems are not only fascinating but also relevant from a practical point of view, essentially because they give information on morphodynamic processes of which they are the occasional visible imprint. The origin of coastal rhythmic patterns has been puzzling scientists for decades but there is nowadays the consensus that they emerge from feedbacks between hydrodynamics and morphology through the sediment transport (Coco & Mur-

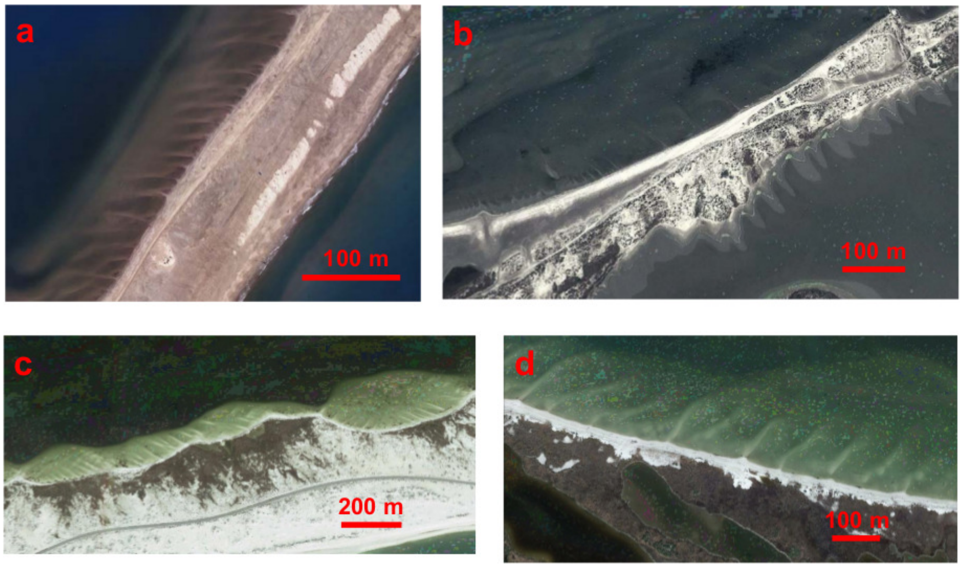

Figure 1. Shore-transverse finger sand bars in coasts with abundant sand supply. a) El Trabucador, Ebro delta, Catalonia, Spain (40° 36' 54" N , 0° 43' 44" E). Source: Catalan Geographic and Geologic Institute, image from 2012. b) Beauduc Beach, Rhône Delta, France (43° 23' 41" N, 4° 34' 35" E). Source: Google Earth, Maxar Technologies, image from 28/04/2010. Notice the bars (of different shape) at both sides of the barrier beach. c) Santa Rosa Island, Florida, USA (30° 22' 06" N, 86° 57' 32" W). Source: Google Earth, Terrametrics, image from 15/01/2018. d) Horn Island, Mississippi, USA (30° 14' 38" N, 88° 41' 06" W). Source: Google Earth, Landsat/Copernicus, image from 27/01/2015. The North in all plots is upward directed.

ray, 2007). Up to now, the self-organization mechanisms related with the sediment transport due to the longshore current and the rip currents have been largely explored while possible feedbacks arising from the cross-shore transport have been systematically ignored (Ribas et al., 2015). In fact, in the existing morphodynamic models the formation of rhythmic patterns occurs on top of a cross-shore profile that is assumed to be essentially in equilibrium. The net cross-shore transport is evaluated in a simplified way such that it only leads to a diffusive term in the equation governing bed evolution. Several studies with such models have been able to successfully describe the genesis of some types of transverse bars observed in nature (Ribas et al., 2015). However, the formation mechanism for transverse finger bars in low-energy environments (Figure 1) remains mostly unexplained. In fact, observational studies on such transverse finger bars show that they develop preferably on gentle sloping beaches with abundant supply of sand (Niederoda & Tanner, 1970), probably with a beach profile above equilibrium (Evans, 1938). In this situation, the cross-shore transport dominates and thereby it might trigger a destabilizing mechanism instead of a damping one. Examples are the transverse finger bars along lake shores (Evans, 1938), estuaries (Eliot et al., 2006), barrier islands (Fig.1c,d) (Gelfenbaum & Brooks, 2003) and delta barrier beaches (Fig.1a,b) like El Trabucador back-barrier system, in the Ebro delta (Mujal-Colilles et al., 2019).

At its south west flank this delta has a long narrow spit, called El Trabucador, and its back-barrier beach is a shallow terrace of 100 m cross-shore up to 0.7 m depth, which face the semi-enclosed Alfacs bay. The sediment is fine sand and is provided by the open sea beach during overwash events. This beach is microtidal and wave energy is typically low due to the small fetch, with maximum heights ~ 0.6 m during NW wind and short

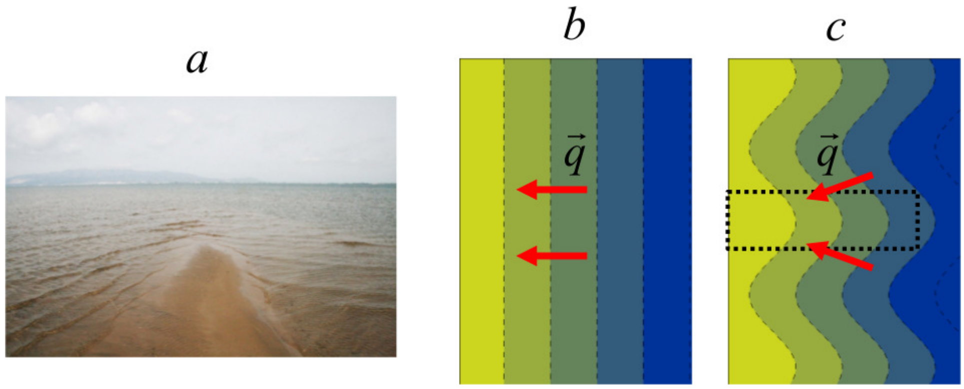

Figure 2. The morphodynamic instability mechanism: a) wave focusing by a shore-transverse sandbar due to topographic refraction in El Trabucador back-barrier beach, b) net onshore sediment transport for rectilinear shore-parallel depth contours above the equilibrium, and c) rotation of the cross-shore sediment flux for curvilinear depth contours and sediment convergence over the shoals (e.g., inside the dotted rectangle). In panels b) and c), yellow/blue colours mean shallow/deep water, respectively.

periods (< 3 s). Nevertheless, wave activity is intense enough to move the fine sand over all the terrace and a system of transverse finger bars is often present (Fig.1a). The alongshore wavelength is variable but the average and the most frequent is 20 m (Mujal-Colilles et al., 2019). The bars are thin and elongated with a cross-shore extent up to some 60 m and they commonly open an anti-clockwise angle of $10° - 40°$ with the shore normal. Field observations and aerial photos show that the system is persistent and dynamic. Typically, waves refract in the proximity of the bars and wave crests cross each other over the bars thereby focusing their energy there (Fig.2a). This process, very noticeable and ubiquitous, was already described by Niederoda and Tanner (1970) as an important process for the formation and maintenance of transverse finger bars in other sites.

In this paper we present a new morphodynamic self-organization mechanism based on the cross-shore transport that could explain the generation of transverse finger bars in shallow terraces. The instability mechanism is described in section 2. Section 3 presents the model runs that confirm that, if the beach profile is above equilibrium, the cross-shore transport can generate shore-transverse sand bars similar to those observed at El Trabucador back-barrier beach. We use a morphodynamic model that has been validated with observations (Arriaga et al., 2017). The concluding remarks are given in section 4, along with the limitations and relevance of the model exercise.

2 The New Instability Mechanism

To describe the instability mechanism we consider an idealized rectilinear beach with an alongshore uniform bathymetry and waves incident normally to the shore. Assume a cross-shore beach profile with a so gentle slope that it is above the equilibrium. Thereby, the gravity-driven transport is small and the net depth-averaged cross-shore sediment flux, $\vec{q}$, is onshore directed, dominated by wave asymmetry and skewness (Figure 2b). Assume now a shoal breaking the alongshore uniformity. The waves propagating in the vicinity of the shoal will refract so that the wave crests at both sides of the shoal will veer towards the shallower part (Figure 2a). As a result, the cross-shore sediment flux will veer towards the shallower region too bringing sediment to it. This will swell the shoal so that a positive feedback will occur (Figure 2c). If the cross-shore profile is so steep that it is below the equilibrium, the net cross-shore transport is dominated by gravity (hence seaward directed) and the situation is just opposed.

The instability mechanism can be mathematically described with an idealized morphodynamic equation associated to the cross-shore transport. This also facilitates understanding the essential differences with the usual approach where the cross-shore transport plays a diffusive role. We consider a Cartesian coordinate system (x, y, z), x pointing seawards, y along the shoreline and z upwards, $z=0$ being the mean sea level. We represent the cross-shore sediment transport as

$$\vec{q} = q_w \frac{\vec{k}}{k} - \gamma \nabla z_b \tag{1}$$

where q_w is the onshore wave-driven transport module, $\vec{k}$ is the wavenumber vector, $\gamma > 0$ is a wave stirring factor and $z = z_b(x, y, t)$ is the bed level. These are the only two terms (the wave-driven and the gravitational) needed to capture the essence of the new instability. Other contributions to cross-shore transport, like undertow or infragravity waves, or the sediment transport by the currents are ignored in this section. We consider the shoreline, $y=0$, and an alongshore uniform bathymetry, $z_b = Z(x)$, as a reference beach state, not necessarily in equilibrium. The local reference beach slope is $\beta(x) = -dZ(x)/dx$. In the reference state we assume shore-normal incident monochromatic waves.

Let us consider now a small alongshore irregularity of the reference state, $h(x, y, t)$, so that $z_b(x, y, t) = Z(x) + h(x, y, t)$. It is important to realize that although h is assumed to be infinitesimal, the perturbation with respect to the equilibrium, $Z(x) - Z_e(x) + h(x, y, t)$ is not. Let θ and ϕ be the (small) angles between ∇z_b and $\vec{k}$ and the $-x$ axis, respectively, that is,

$$\nabla z_b = |\nabla z_b|(-\cos\theta\, \hat{e}_x + \sin\theta\, \hat{e}_y) \quad , \qquad \vec{k} = k(-\cos\phi\, \hat{e}_x + \sin\phi\, \hat{e}_y) \tag{2}$$

where $\hat{e}_x, \hat{e}_y$ are the unit vectors along the x, y axes. Introducing this in the sediment transport one obtains

$$\vec{q} = q_w^0(-\cos\phi\, \hat{e}_x + \sin\phi\, \hat{e}_y) + \gamma^0 \beta\, \hat{e}_x - \gamma^0 \nabla h \tag{3}$$

where q_w^0 and γ^0 are the magnitudes of the wave-driven transport and the stirring in the reference state. The perturbations in q_w and γ have been here neglected for simplicity, as done in most morphodynamic models (Ribas et al., 2015). Then, by keeping only zero and first order terms,

$$\vec{q} = Q\, \hat{e}_x + q_w^0\, \phi\, \hat{e}_y - \gamma^0 \nabla h \tag{4}$$

with $Q = \gamma^0 \beta - q_w^0$ being the net transport in the reference state. Due to topographic refraction, the wave fronts tend to become parallel to the depth contours. We can therefore assume $\phi = \mu\, \theta$ with $0 < \mu(x, y) < 1$. In fact, $\phi(x, y)$ is not a local function of $\theta(x, y)$, since it depends on the whole wave refraction from offshore to the (x, y) location, but for our purpose and for small angles this assumption seems reasonable. Furthermore, to first order, equation (2) leads to

$$\theta = \frac{1}{\beta} \frac{\partial h}{\partial y} \tag{5}$$

Finally, by invoking the sediment conservation equation:

$$\frac{\partial z_b}{\partial t} + \frac{1}{1-p} \nabla \cdot \vec{q} = 0 \tag{6}$$

with p being the bed porosity, one obtains the following morphodynamic governing equation:

$$(1-p)\frac{\partial h}{\partial t} = \frac{\partial}{\partial x}\left(\gamma^0 \frac{\partial h}{\partial x}\right) + \frac{\partial}{\partial y}\left(\gamma^0 (1-\alpha) \frac{\partial h}{\partial y}\right) - \frac{dQ}{dx} \tag{7}$$

where $\alpha = \mu q_w^0/(\gamma^0\beta)$. This is a diffusion equation where the cross-shore and the alongshore diffusivities are γ^0 and $\gamma^0(1-\alpha)$, respectively. If the reference state is an equilibrium one, $Q = 0$, and wave refraction is neglected, $\mu = 0$, both diffusivities in the governing equation (7) are equal and positive. This is the standard approach in which any bathymetric perturbation tends to damp (Ribas et al., 2015). Including wave refraction reduces the alongshore diffusivity but, if the reference state is an equilibrium one, the alongshore diffusivity is still positive. However, if the reference profile is above equilibrium, the net cross-shore transport is positive, $q_w^0 > \gamma^0\beta$ and the the alongshore diffusivity may become negative. In this case, alongshore irregularities can grow by instability.

3 Morphodynamic Model Runs

3.1 Brief Model Description

To study in more detail how the instability mechanism works and is able of generating alongshore rhythmic morphology we use the so-called Q2Dmorfo model (Arriaga et al., 2017). This model computes the evolving bathymetry in a rectangular domain under certain wave forcing. The main inputs are the initial bathymetry, the wave forcing and an assumed equilibrium beach profile. From this, the model computes the wave field inside the domain and the sediment flux, and it updates the bathymetry at each time step from the sediment conservation equation (6). The model is similar to other existing 2DH morphodynamic models except that it computes the sediment flux directly from the wave field in a parametric way without resolving the surf zone hydrodynamics. By paying the price of missing some important surf zone processes (like rip currents) it is able to describe the large scale coastal evolution at time scales of decades-centuries. Although we are here interested in length scales much smaller than those for which the model is designed, we use it for two reasons. First, it describes the cross-shore transport as proportional to the deviation of the local beach slope with respect to the equilibrium one. Second, it filters out the rip current circulation which is another known factor of alongshore rhythmic morphology. Therefore, the mechanism associated to the cross-shore transport can be analyzed in isolation.

The model is here briefly described, mainly indicating how the sediment fluxes are calculated from the wave field. More details can be found in Arriaga et al. (2017). We use the same coordinate system introduced in section 2 and a computational domain $0 \leq x \leq L_x, 0 \leq y \leq L_y$, including emerged and submerged beach. The depth-integrated sediment flux is decomposed into three components,

$$\vec{q} = \vec{q}_L + \vec{q}_C + \vec{q}_D \tag{8}$$

The first one is a parameterization of the longshore sediment flux driven by the breaking waves. The second one is the cross-shore transport and reproduces the tendency of the beach to evolve towards the equilibrium profile. The third term is an alongshore diffusive transport to account for the hydrodynamic smoothing of small scale bathymetric noise. The cross-shore and alongshore directions for an undulating coast loose the clear meaning they have for a rectilinear coast. However their meaning can be recovered from the mean trend of the bathymetric contours if the small scale bathymetric features are filtered out. Also, these averaged contours are those felt by wave propagation and transformation. Therefore, from the actual bathymetry, $z_b(x, y, t)$, an averaged bathymetry, $\bar{z}_b(x, y, t)$, is defined by using a running average in a rectangular window of size a_x and a_y, which are at least of the order of the wavelength. Then, we define the local mean "cross-shore" direction by the unit vector

$$\hat{n} = -\frac{1}{|\nabla \bar{z}_b|}\nabla \bar{z}_b \tag{9}$$

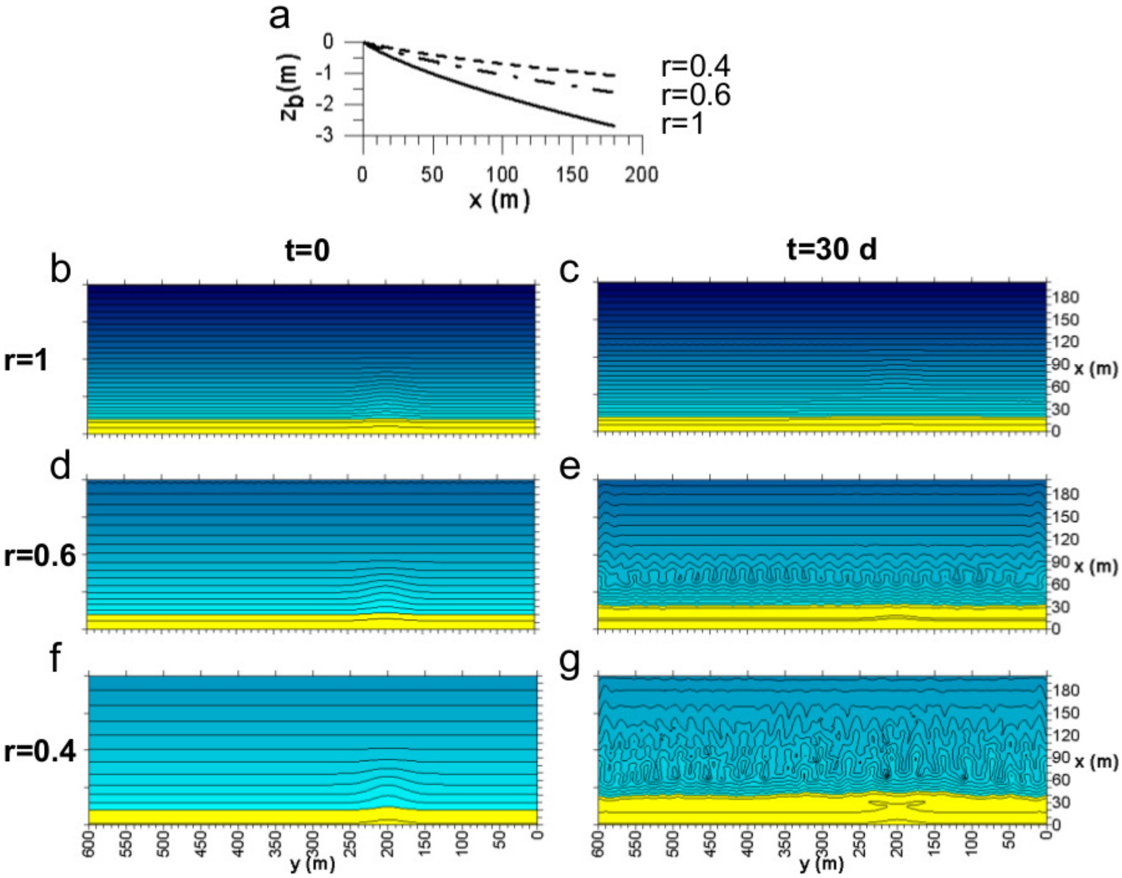

Figure 3. Sensitivity to the initial beach slope: a) Initial profile for $r = 1$ in solid line (which is also the equilibrium profile), and for $r = 0.6$ and $r = 0.4$, and b)-g) Q2Dmorfo result for the three r values. Panels b), d) and f) are the initial bathymetry and panels c), e) and g) are the bathymetries at $t = 30$ d. Yellow and blue colours represent the emerged and submerged beach, respectively, and depth contours are plotted every 0.1 m.

The cross-shore transport in equation (8) is proportional to the difference between the local equilibrium slope, $\beta_e(D)$, and the actual slope in the local cross-shore direction,

$$\vec{q}_C = -\gamma_C(\hat{n} \cdot \nabla z_b + \beta_e)\,\hat{n} \tag{10}$$

The water depth is $D = -z_b$ and $\gamma_C(D)$ is a wave stirring factor. The depth where γ_C magnitude is 0.02 times its shoreline value is the depth of closure, D_c. Note that equation (10) implies that the wave-driven transport is up-slope the averaged bathymetry which, in the framework of section 2, is equivalent to the limit case $\mu = 1$, that is, $\phi = \theta$.

Model runs are done keeping in mind the geometry and typical wave conditions at El Trabucador back-barrier beach. A rectangular domain $L_x = 200$ m (cross-shore), $L_y =$ 600 m (longshore), with a dry beach width of 20 m. As equilibrium profile, we consider a shifted Dean profile (Falqués & Calvete, 2005)

$$Z_e(x) = -B\left((x + x_0)^{2/3} - x_0^{2/3}\right) \tag{11}$$

The parameters, $B = 0.095$ m$^{1/3}$ and $x_0 = 9.42$ m, are chosen to obtain a shoreline slope $\beta_s = 0.03$ and to approximate a Dean profile far from the shoreline, $Z_d = -Ax^{2/3}$, with

$A = 0.084$ m$^{1/3}$ (value coherent with a sediment grain size of $d_{50} \approx 0.15$ mm (Dean & Dalrymple, 2002)). The imposed values for β_s and d_{50} are obtained from El Trabucador data (Mujal-Colilles et al., 2019). The initial bathymetry for the model runs is

$$z_b(x, y, 0) = rZ_e(x) + h(x, y) \tag{12}$$

where $h(x, y)$ is a small localized perturbation and r controls whether the initial profile is above ($r < 1$) or below ($r > 1$) equilibrium (Figure 3a,b). A value $r \approx 0.4$ is obtained when the shifted Dean profile to the observed profile at El Trabucador, and it is used as default value. It also indicates that the observed profile is clearly above the equilibrium profile that would correspond to its grain size. As default wave forcing we use constant wave conditions characteristic from El Trabucador, $H_s = 0.28$ m, $T_p = 2$ s (Mujal-Colilles et al., 2019), and shore-normal incidence, $\theta = 0$. The default bathymetric smoothing box is $a_x = 3$ m and $a_y = 10$ m, and the closure depth is estimated out of the data, $D_c = 0.8$ m. The spatial grid is defined by $dx = 0.5$ m and $dy = 1.5$ m and the time step is $dt = 0.00002$ d.

3.2 Model Results

For $r = 1$ the initial perturbation tends to smooth out and the bathymetric contours become rectilinear and parallel to the shoreline (Figure 3b,c). The initial morphology is clearly stable. In contrast, for $r = 0.4$ undulations develop in the depth contours (Figure 3f,g). Quite rapidly, the amplitude of the undulations increases and a complex bathymetry encompassing shore-transverse bars appears in the shoaling zone. Thus, the initial morphology is clearly unstable. At some spots, the morphology is relatively regular but at others it is quite complex with several length scales. However, an alongshore length scale $L \approx 25$ m becomes apparent. Also, the shoreline progrades, which is consistent with the beach being under accretive conditions. A detailed description of the time evolution of the morphology in the default case can be found in the Supporting Information. For $r = 0.5 - 0.7$ something similar occurs but at a slower rate as r increases. For $r = 0.7$ only some weak undulations in the depth contours have developed after 30 days. In contrast, the behaviour for $r = 0.8$ is similar to $r = 1$. Thus, it is found that the instability develops if the profile is above equilibrium but with a certain threshold.

To discard that the instability is a numerical artifact, the sensitivity to the numerical parameters is investigated. Little sensitivity is found by taking $dy = 0.5 - 1.5$ m or changing the size of the domain, $L_y = 300 - 600$ m. Also results do not depend on the initial perturbation (three cases have been analysed, see the Supporting Information for details). The particular morphology is somewhat different, but the qualitative behaviour is the same. The sensitivity to the averaging box size, a_x, a_y, has been carefully examined. It is found that a_x hardly influences the results but a_y has a strong influence on the shape and wavelength of the transverse bar system. For small a_y the morphology is quite complex and noisy, and the spacing between the bars is small. In contrast, as a_y increases, it becomes smoother and the spacing increases (see Figure 4a,b). Indeed, it is found that wavelength increases (roughly) linearly with a_y (see the Supporting Information for details). For $a_y > 50$ m, bars do not grow inside the domain. The dependence of the results on a_y is discussed in Section 4.

Regarding the wave conditions, the values $H_s = 0.14 - 0.42$ m and $T_p = 1 - 3$ s are tested and results hardly change (more details in the Supporting Information). More influence have D_c and θ. The values $D_c = 0.6 - 1.2$ m have been examined and its primary influence is an increase of the cross-shore length of the bars with increasing D_c (Figure 4c,d). It is seen that for oblique wave incidence, bars grow faster and tend to be aligned against the wave incidence (Figure 4e,f). Morphodynamic noise appears much sooner than for shore normal wave incidence and the model breaks down earlier (for example at $t = 15$ d for $\theta = 10°$ but as soon as $t = 2$ d for $\theta = 40°$).

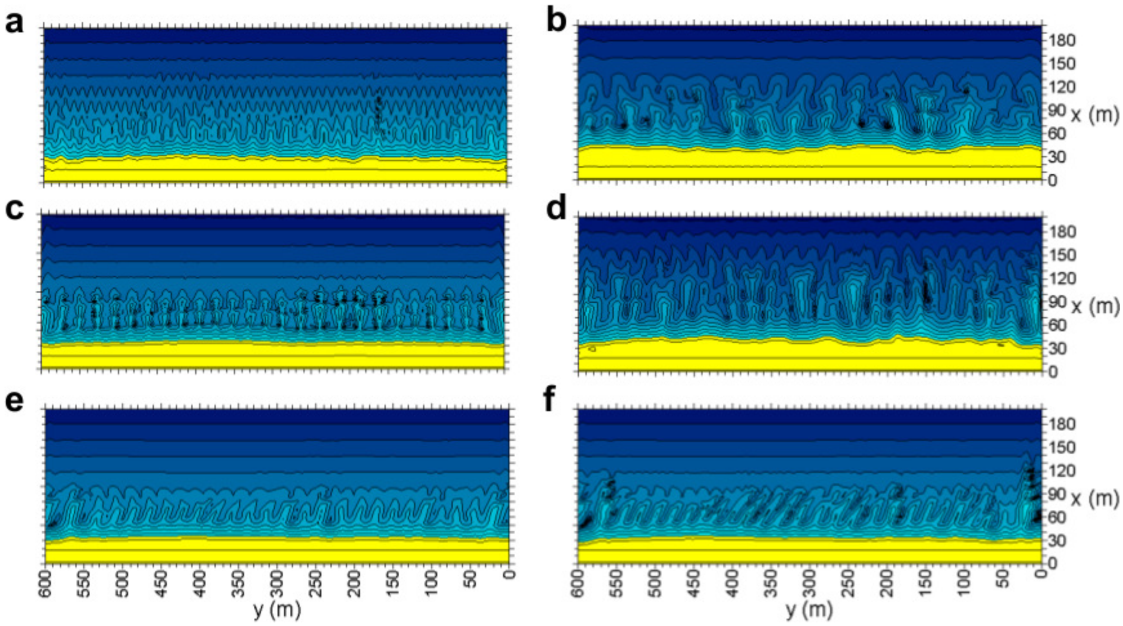

Figure 4. Q2Dmorfo result for (a) $a_y = 5$ m and (b) $a_y = 20$ m, both at $t = 20$d, for (c) $D_c = 0.6$ m and (d) $D_c = 1$ m, both at $t = 19$ d, and for (e) $\theta = 10°$ and (f) $\theta = 20°$, both at $t = 2$ d. The other parameters have their default values. Yellow and blue colours represent the emerged and submerged beach, respectively, and depth contours are plotted every 0.1 m. In case of non shore-normal wave incidence, waves came from the right on the plot.

4 Final Remarks

The resulting onshore sediment transport on beaches that are significantly shallower than the equilibrium bathymetric profile can produce an instability that breaks the alongshore uniformity. This mechanism can explain the quite common existence of transverse finger bars in shallow areas with an abundant supply of sand in delta barrier beaches, barrier islands and estuaries. The instability occurs because wave refraction rotates the wave fronts towards the growing transverse bars so that the onshore transport veers too and causes flux convergence over the bars.

It is remarkable that, despite the present modelling approach is just meant to capture the essence of the instability in a qualitative way, the modelled morphology bears a reasonable similitude with the transverse bars shown in Figure 1. Moreover, the model application to El Trabucador gives emerging length scales which are consistent with those observed in this site. The dominant alongshore spacing between the bars, L, increases linearly with the alongshore length of the smoothing box, a_y. The latter must be of the order of the minimum alongshore length scale of the bathymetric features that can affect wave refraction, which is difficult to ascertain but must be of the order of the wavelength of the wave forcing. At the water depths $D \approx 0.4 - 0.6$ m where the bars form, waves with $T_p = 2 - 3$ s have wavelengths in the range $4 - 7$ m which would be an appropriate range for a_y too. Alongshore wavelengths $L \approx 16 - 19$ m are then obtained, which are consistent with the most frequent bar spacing at El Trabucador. Regarding the cross-shore extent of the bars, it is controlled by the depth of closure, D_c, and a value of about $60 - 90$ m is found for this site (the maximum observed one is about 60 m).

Although we have focused here on illustrating the capability of the present mechanism to generate transverse finger bars in areas of sand excess it could also influence the down-state sequence under accretive conditions in any beach (Wright & Short, 1984) and the development of, e.g., crescentic bars (Dubarbier et al., 2017). This should be investigated with a surf (and shoaling) zone morphodynamic model incorporating a parameterization of cross-shore transport capable of accounting for the present instability mechanism in open ocean beach environments.

The instability concept had been applied to explain the formation of beach cusps (Dodd et al., 2008), crescentic bars (Garnier et al., 2008), shore-transverse bars (Ribas et al., 2012), shoreline sand waves and large scale cuspate features (and spits) (Ashton et al., 2001). In all these cases the morphological features develop out of an equilibrium state, i.e., time invariant, both in the case of linear or nonlinear analysis. In contrast, the new instability develops from a morphology which is necessarily not an equilibrium state. In this sense, it is a finite-amplitude instability, i.e., it can not be captured by the usual linear stability analysis of an equilibrium morphology. Finite-amplitude instabilities are common in other fields of Physics (Drazin & Reid, 1981; Grossmann, 2000; Eckhardt et al., 2007) but, to our knowledge, they had not been found so far in coastal geomorphology.

Acknowledgments

Datasets from El Trabucador back-barrier beach are included in this paper: Mujal-Colilles et al. (2019) This research is part of the Spanish Government projects CTM2015-66225-C2-1-P and RTI2018-093941-B-C33 (MINECO/FEDER). .

References

Amoudry, L. O., & Souza, A. J. (2011). Deterministic coastal morphological and sediment transport modeling: A review and discussion. *Reviews of Geophysics*, *49*(2). doi: 10.1029/2010RG000341

Arriaga, J., Rutten, J., Ribas, F., Ruessink, B., & Falqués, A. (2017). Modeling the longterm diffusion and feeding capability of a mega-nourishment. *Coast. Eng.*, *121*, 1-13.

Ashton, A., Murray, A. B., & Arnault, O. (2001). Formation of coastline features by large-scale instabilities induced by high-angle waves. *Nature*, *414*, 296-300.

Coco, G., & Murray, A. B. (2007). Patterns in the sand: From forcing templates to self-organization. *Geomorphology*, *91*(271-290).

Dean, R. G., & Dalrymple, R. A. (2002). *Coastal processes.* Cambridge: Cambridge University Press.

Dodd, N., Stoker, A., Calvete, D., & Sriariyawat, A. (2008). On beach cusp formation. *J. Fluid Mech.*, *597*, 145-169.

Drazin, P. G., & Reid, W. H. (1981). *Hydrodynamic Stability.* Australia: Cambridge University Press.

Dubarbier, B., Castelle, B., Ruessink, G., & Marieu, V. (2017). Mechanisms controlling the complete accretionary beach state sequence. *Geophys. Res. Lett.*, *44*. (doi:10.1002/2017GL073094)

Eckhardt, B., Schneider, T. M., Hof, B., & Westerweel, J. (2007). Turbulence transition in pipe flow. *Ann. Rev. Fluid Mechanics*, *39*, 447-468.

Eliot, M. J., Travers, A., & Eliot, I. (2006). Morphology of a Low-Energy Beach, Como Beach, Western Australia. *J. Coastal Res.*, *22*(1), 63-77.

Evans, O. F. (1938). The classification and origin of beach cusps. *J. Geology*, *46*, 615-627.

Falqués, A., & Calvete, D. (2005). Large scale dynamics of sandy coastlines. Diffusivity and instability. *J. Geophys. Res.*, *110*(C03007). (doi:10.1029/2004JC002587)

Fernández-Mora, A., Calvete, D., Falqués, A., & de Swart, H. E. (2015). Onshore sandbar migration in the surf zone: New insights into the wave-induced sediment transport mechanisms. *Geophysical Research Letters*, *42*(8), 2869-2877. doi: 10.1002/2014GL063004

Garnier, R., Calvete, D., Falqués, A., & Dodd, N. (2008). Modelling the formation and the long-term behavior of rip channel systems from the deformation of a longshore bar. *J. Geophys. Res.*, *113*(C07053). (doi:10.1029/2007JC004632)

Gelfenbaum, G., & Brooks, G. R. (2003). The morphology and migration of transverse bars off the west-central florida coast. *Mar. Geol.*, *200*, 273-289.

Grossmann, S. (2000). The onset of shear flow turbulence. *Reviews of Modern Physics*, *72*(2), 603-618.

Mujal-Colilles, A., Grifoll, M., & Falqués, A. (2019). Rhythmic morphology in a microtidal low-energy beach. *Geomorphology*, *334*, 151-164. doi: doi.org/10.1016/j.geomorph.2019.02.037

Niederoda, A. W., & Tanner, W. F. (1970). Preliminary study on transverse bars. *Mar. Geol.*, *9*, 41-62.

Ribas, F., de Swart, H. E., Calvete, D., & Falqués, A. (2012). Modeling and analyzing observed transverse sand bars in the surf zone. *J. Geophys. Res.*, *117*(F02013). (doi:10.1029/2011JF002158)

Ribas, F., Falqués, A., de Swart, H. E., Dodd, N., Garnier, R., & Calvete, D. (2015). Understanding coastal morphodynamic patterns from depth-averaged sediment concentration. *Rev. Geophys.*, *53*. (doi:10.1002/2014RG000457)

Wright, L. D., & Short, A. D. (1984). Morphodynamic variability of surf zones and beaches: A synthesis. *Mar. Geol.*, *56*, 93-118.

Figure 1.

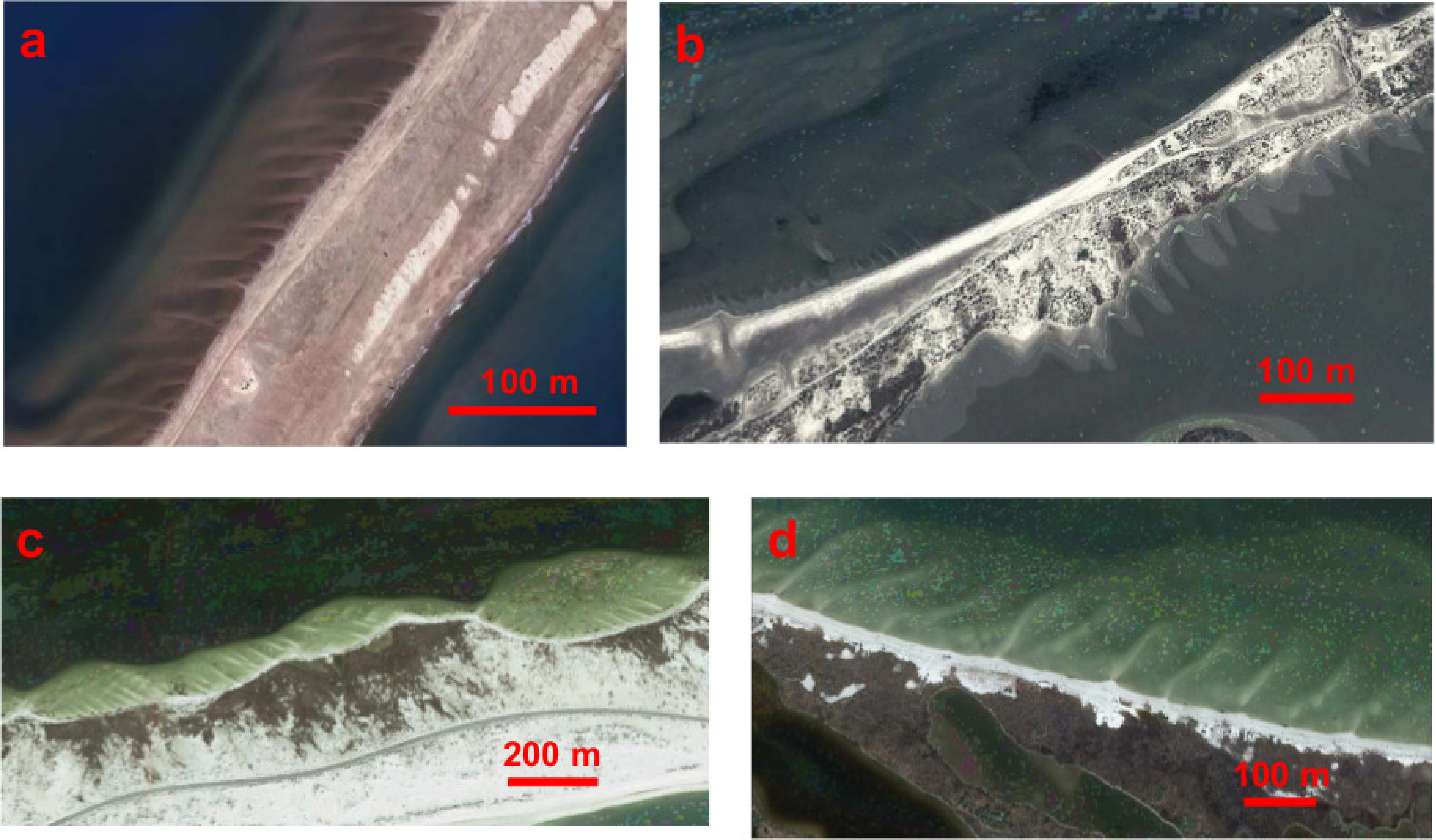

a
100 m
b
100 m
c
200 m
d
100 m

Figure 2.

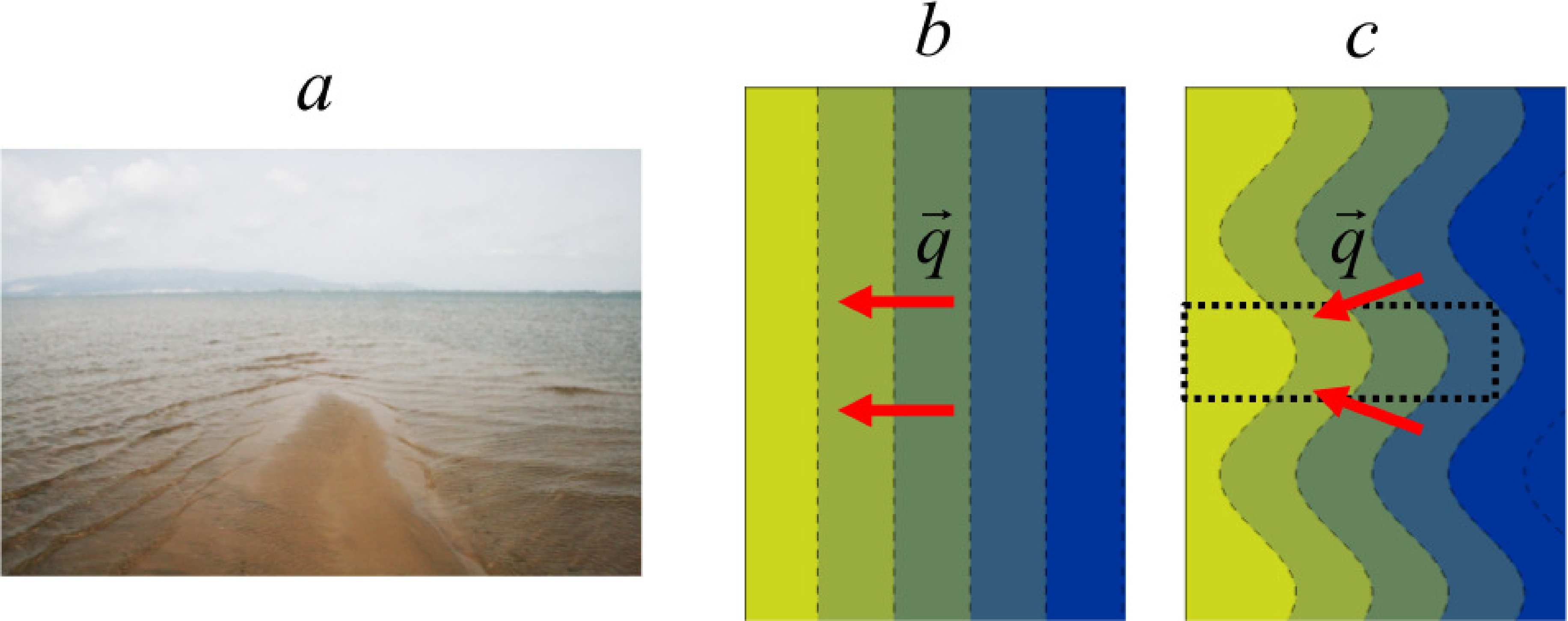

a
b
c
$\vec{q}$
$\vec{q}$

Figure 3.

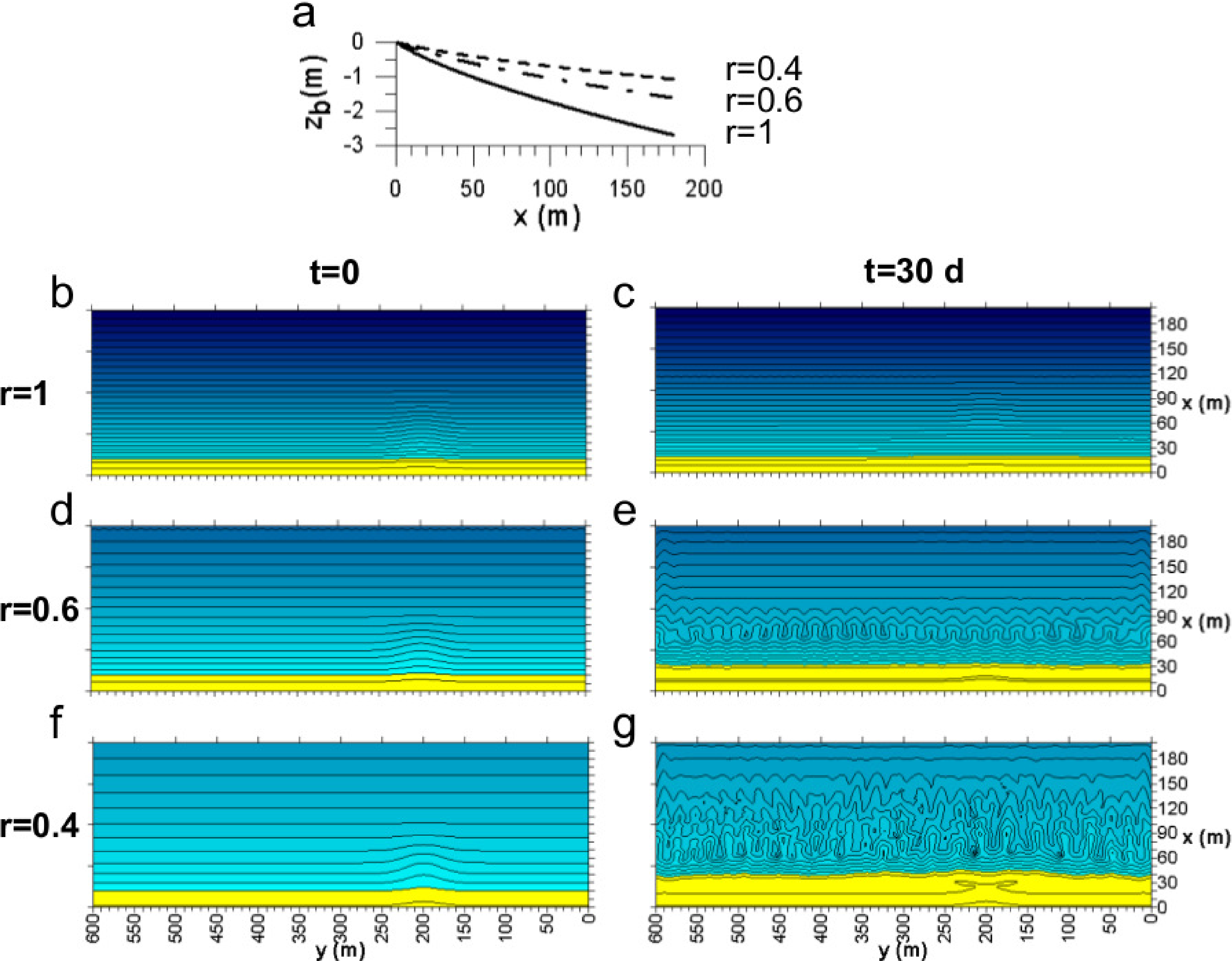
a
r=0.4
r=0.6
r=1
z_b(m)
x (m)
t=0
t=30 d
b
c
d
e
f
g
r=1
r=0.6
r=0.4
x (m)
y (m)

Figure 4.

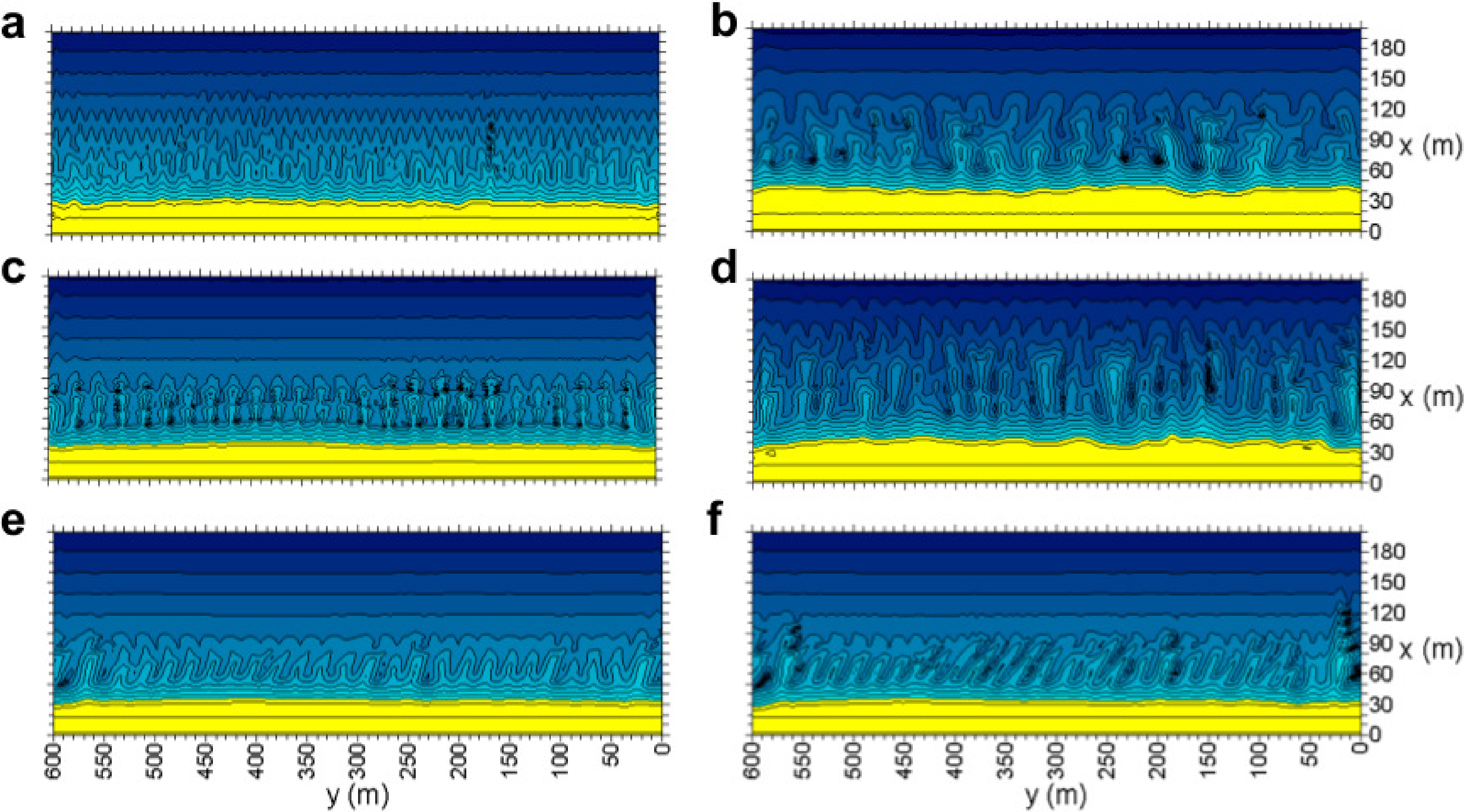

a
b
c
d
e
f
180
150
120
90
60
30
0
x (m)
600
550
500
450
400
350
300
250
200
150
100
50
0
y (m)

Supporting Information for "A new morphodynamic instability associated to the cross-shore transport in the nearshore"

A. Falqués[1], F. Ribas[1], A. Mujal-Colilles[2] and C. Puig-Polo[3]

[1]Physics Department, Universitat Politècnica de Catalunya, Campus Diagonal Nord, C. Jordi Girona, 1-3, 08034 Barcelona, Catalonia, Spain

[2]Department of Nautical Sciences and Engineering, Universitat Politècnica de Catalunya

[3]Department of Civil and Environmental Engineering, Universitat Politècnica de Catalunya

Contents of this file

Introduction

In this Supporting Information document, some results are described in more detail, with the help of the three extra figures S1-S3 and the four extra text paragraphs S1-S4. Text S1-S3 describe results that are shown in Figures S1-S3, respectively. Text S4 describe results that are not illustrated by any Figure.

Figure S1. Default simulation: time development of the instability for $r = 0.4$. Depth contours every 0.1 m. Alongshore and cross-shore coordinates in m. Yellow and blue colours represent the emerged and submerged beach, respectively.

Text S1. Figure S1 shows the time development of the instability for $r = 0.4$ from a small localized perturbation (default simulation). Initially, the bathymetry evolves quickly near the perturbation, where a couple of transverse bars form. Also, undulations form near the lateral boundaries ($t = 1$ d). Gradually, the instability spreads through all the domain in the shoaling zone giving rise to transverse bars. At some spots, the morphology is relatively regular but at others it is quite complex with several lenght scales. Also, the signal of the initial perturbation is lost as time goes on. During some time lapses, the morphological changes seem to slow down (e.g., between $t = 3$ d and $t = 4$ d). The shoreline progrades but not uniformly, small alongshore undulations develop. In general, the model runs stop after some time. This happens when some sand bar rises above sea level as the model does not include the processes that govern this situation in nature. Sometimes, unrealistically deep troughs or morphodynamic noise develop as the processes that in nature would counteract the positive feedback are not included by our idealized model. Nevertheless, the model successfully describes the existence or not of positive feedback and the morphology that tends to emerge. Of course, the final steps before model breakdown must be regarded with care. Interestingly, this breakdown occurs in general after a time long enough to elucidate the main characteristics of the emerging morphology. For example, for the default simulation, this occurs after $t = 60$ d.

Figure S2. Morphology for $t = 10$ d starting with different initial conditions: a) small bump on the shoreline, b) noise from the lateral boundaries and c) random bathymetric perturbations. Depth contours every 0.1 m. Yellow and blue colours represent the emerged and submerged beach, respectively.

Text S2. Figure S2 shows the morphology for $t = 10$ d and for different initial perturbations: an undulation in the shoreline, small noise from the lateral boundaries and random perturbations distributed inside the domain. In all cases, although the details of the time evolution may be different, the final morphology encompasses transverse bars with a similar alongshore wavelength of 21 m. The final morphology for the two first cases is quite similar but for the random perturbation the morphology is more irregular and intricate.

Figure S3. Four panels at the top: morphology at $t = 20$ d and for different alongshore sizes, a_y, of the averaging box for the bathymetry. Depth contours every 0.1 m. Yellow and blue colours represent the emerged and submerged beach, respectively. Panel at the bottom: dependence of the alongshore wavelength of the bar system on a_y.

Text S3. The alongshore size, a_y has a strong influence on the shape and wavelength of the transverse bar system, as seen in Figure S3. For small a_y the morphology is quite complex and noisy, and the spacing between the bars is small. In contrast, as a_y increases, it becomes smoother and the spacing increases. It is found that the wavelength increases roughly linearly with a_y, $L \approx 10 + 1.3\, a_y$ (in m). For $a_y = 50$ m, few bars form and it is hard to identify their spacing. For even larger a_y, the bars do not grow inside the domain, only some undulation or some noise near the lateral boundaries become apparent.

Text S4. It is found that T_p has almost no direct influence on the instability, the morphology after 10 d being very similar for $T_p = 1, 2, 3$ s. It seems that the wavelength of the bars tends to slightly grow with T_p. Notice, however, that T_p affects indirectly the bar spacing because the appropriate a_y depends on the wavelength of the wave forcing. The shape of the bars is also similar by varying H_s $(0.14, 0.28, 0.42$ m), although their cross-shore length increases with H_s and the wavelength tends to increase too.

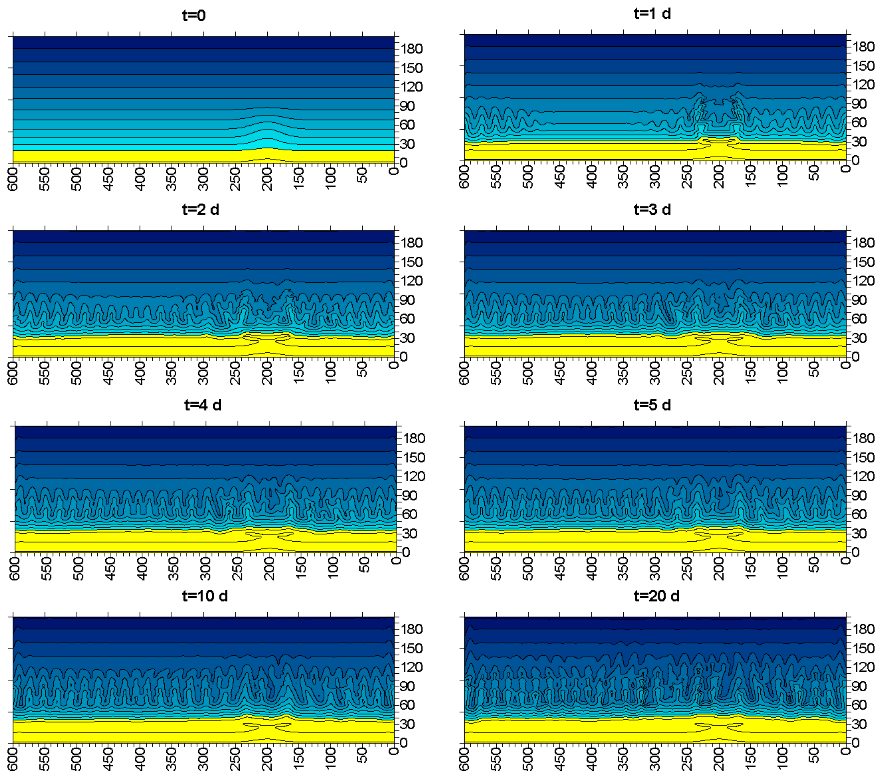

Figure S1. Default simulation: time development of the instability for $r = 0.4$. Depth contours every 0.1 m. Alongshore and cross-shore coordinates in m. Yellow and blue colours represent the emerged and submerged beach, respectively.

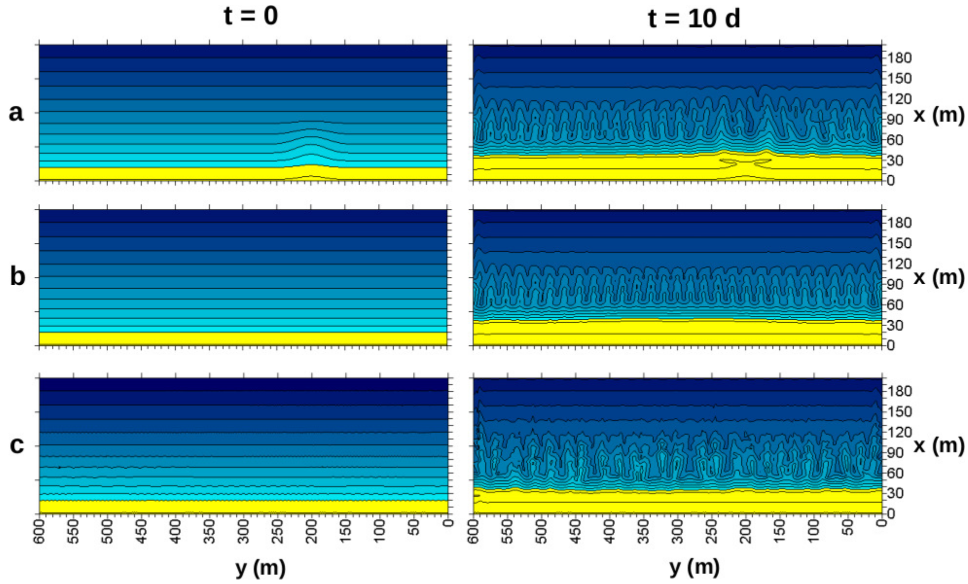

Figure S2. Morphology at $t = 10$ d starting with different initial conditions: a) small bump on the shoreline, b) noise from the lateral boundaries and c) random bathymetric perturbations. Depth contours every 0.1 m. Yellow and blue colours represent the emerged and submerged beach, respectively.

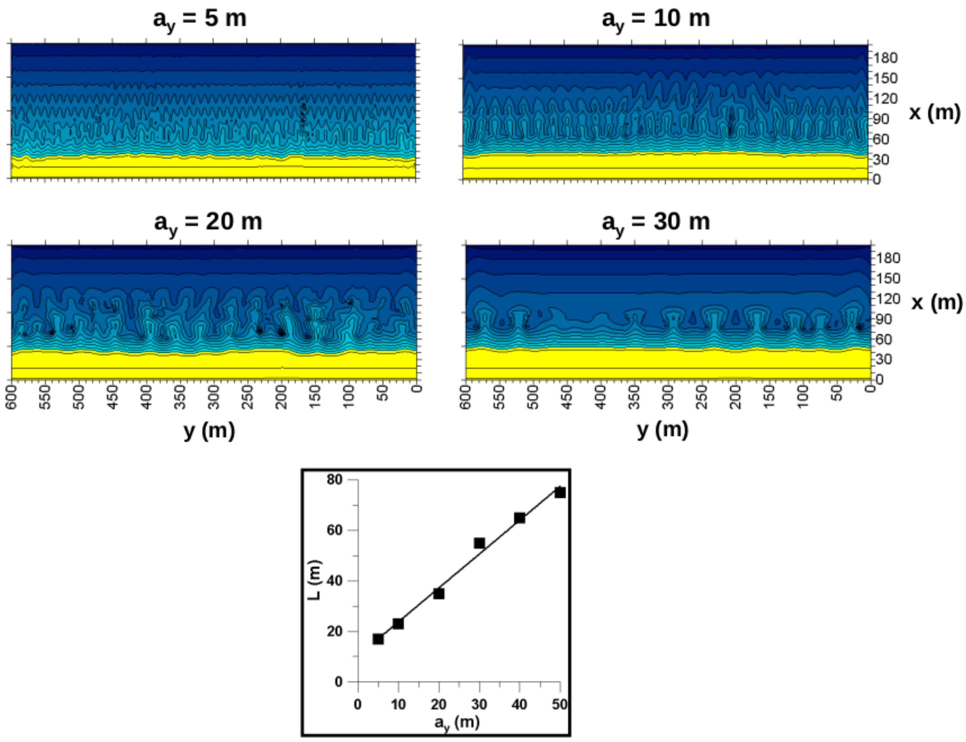

Figure S3. Four panels at the top: morphology at $t = 20$ d and for different alongshore sizes, a_y, of the averaging box for the bathymetry. Depth contours every 0.1 m. Yellow and blue colours represent the emerged and submerged beach, respectively. Panel at the bottom: dependence of the alongshore wavelength of the bar system on a_y.